Astron. Astrophys. 321, 397–408 (1997)

ASTRONOMY
AND
ASTROPHYSICS

The extended narrow line region in Mkn 79

II. Modelling

L.S. Nazarova, P.T. O'Brien, and M.J. Ward

Department of Physics & Astronomy, University of Leicester, University Road, LE1 7RH, Leicester, UK

Received 2 July 1996 / Accepted 22 October 1996

Abstract. We present photoionization modelling of the Extended Narrow Line Region (ENLR) in Mkn 79 based on long-slit spectra presented in our previous paper (Nazarova et al. 1996). The ENLR has been modelled with two gas components: a system of high density clouds embedded in a low density gas envelope. The ENLR line fluxes have been calculated allowing for attenuation of the nuclear ionizing continuum as a function of distance from the centre. The diffuse continuum emission from the low density gas is also included as an important secondary source of ionization. We show that this multi-component gas model can successfully reproduce the observed line fluxes and line ratios in the ENLR of Mkn 79 assuming a central source luminosity of 6.6×10^{52}photons s^{-1}, consistent with the dereddened nuclear luminosity. The predicted reflected continuum from the ENLR gas is also in agreement with the observed extended blue continuum emission.

Key words: galaxies: active – galaxies: individual: Mkn 79 – galaxies: Seyfert

1. Introduction

The idea that the difference between Seyfert 1 and Seyfert 2 galaxies is due to varying degree of obscuration and orientation (Antonucci & Miller 1985; Antonucci 1993) has been around for several years, and is strong evidence that Active Galaxies radiate anisotropically (Pogge 1988; Colina 1992). There is also alignment between the radio and Extended Narrow Line Region (ENLR) structure (Unger et al. 1987; Wilson, Ward & Haniff 1988; Haniff et al. 1988; 1991). About 16 galaxies have had their ENLR studied in detail (see compilations in Wilson & Tsvetanov, 1994 and Binette et al. 1996). In our previous paper (Nazarova, O'Brien & Ward, 1996, hereafter Paper 1) we presented ENLR observational data for another object – Mkn 79. In Paper 1 we discussed the ENLR emission at different distances from the centre in two position angles, one along the radio jet (PA=12^o) and one (PA=50^o) in a direction coincident with the stellar bar. We also used emission line ratio diagnostic diagrams to show that the distant regions are characterised by high excitation line ratios which are usually associated with AGN Narrow Line Regions (Veilleux & Osterbrock 1987). In this paper we analyse the observed ENLR emission in Mkn 79 in more detail. Using a photoionization code, multi-component gas models are fitted to the observed ENLR line emission in Sects. 2 and 3. We show in Sect. 4 that the model which fits the line emission can also explain the observed extended blue continuum emission along PA=12^o. The conclusions are given in Sect. 5.

Send offprint requests to: P.T. O'Brien

2. Preliminary analysis of the ENLR emission spectra

The ENLR in Mkn 79 has a more prominent extended structure in the high ionization [OIII]λ5007 line along PA=12^o than along PA=50^o (Paper 1). As discussed in Paper 1, the ENLR spectra were extracted in each position angle using 8 increments(4 arcsec wide) placed symmetrically around a central nuclear extraction window 2 arcsec wide.

A useful and widely used method for the interpretation of emission spectra is that of line ratio diagnostic diagrams, e.g. Baldwin et al. (1981); Robinson et al. (1987). These diagrams plot different line flux ratios and give a visual indication of the dominant mechanism for gas heating and ionization. In Paper 1 we presented several such diagnostic diagrams, but in order to obtain detailed information on the physical conditions of the gas and the photoionizing continuum we now model the emission line spectrum.

The spectra of the nucleus and the ENLR in Mkn 79 as well as in other galaxies where the ENLR has been studied show both high-excitation lines, such as [OIII]$\lambda\lambda$4959,5007 up to [NeV]λ3425, and low excitation lines, such as [OII]$\lambda\lambda$3727, [NII]$\lambda\lambda$6548,6583 and [SII]$\lambda\lambda$6717,6731. Single component models fail to simultaneously fit both high and low excitation line ratios (e.g. Viegas & de Gouveia Del Pino, 1992), leading to the suggestion that the ENLR must be modelled using several gas components, consisting of what are essentially HII regions and a more distributed, highly ionized low density gas component (Evans & Dopita, 1986; Binette et al., 1996).

In Paper 1 the electron temperature and electron density were reliably determined only in the nucleus. The electron temperature in the nucleus estimated using the ratio [OIII]λ4363/[OIII]$\lambda\lambda$5007,4959 implied a temperature of 25000K$\pm$5000K, in agreement with Oke and Lauer (1979). The electron density in the nucleus was derived using the density-sensitive [SII]λ6717/[SII]λ6731 line ratio implying a value $\approx$ 600 cm^{-3}. From this line ratio we also determined that the electron density in the ENLR declined with distance to $<$ 80 cm^{-3} at 7 kpc from the centre. The ENLR electron temperature could not be determined as the [OIII]λ4363 line could only be detected close to the nucleus. Only the [OII]λ3727, [OIII]$\lambda\lambda$4959,5007, [NII]λ λ6548,6583 and [SII]$\lambda\lambda$6717,6731 lines are clearly detected in all 8 regions in our long-slit spectra.

Tables 1 and 2 present the fluxes of the [OII] $\lambda\lambda$3736,3729, [OIII]$\lambda\lambda$4959,5007, [SII]$\lambda\lambda$6717,6731 and [NII]$\lambda\lambda$6548,6583 doublets relative to $H\beta$ for the two position angles, with 1σ errors . The tables also summarize some relevant information from Paper 1. The flux of the Hβ line is given in two ways: the observed flux at the Earth and the emitted flux from one cm^{-2} at source. The mass of the ionized gas has been obtained as a function of the Hβ luminosity L(Hβ) taking the Balmer decrement to be 2.7 (Colina 1992),

M_{gas}=1.64 $\times 10^{-33}$ L(Hβ) N_e^{-1} $M_\odot$.

The average density (N_e) used in this formula and in Tables 1 and 2 was obtained from the [SII]λ6717/[SII]λ6731 line ratio.

Penston et al. (1990) showed that the [OIII]/[OII] line ratio is sensitive to the ionization parameter U. We computed this line ratio as a function of U using the CLOUDY photoionization code (version c8412a, Ferland 1991) for plane parallel slabs of gas with constant density N_e=100 cm^{-3}. Photoionization models were calculated for both powerlaw ($f_\nu \propto \nu^\alpha$, α=$-$1.5 and $-$0.75) and blackbody (T=1.3$\times 10^5$K) nuclear continua. As a blackbody continuum with this temperature has a similar mean ionizing photon energy to a powerlaw continuum with α=$-$1.5 at approximately 35eV, they produce similar ENLR line flux ratios which are in agreement with the typical observed spectra of AGN (Robinson et al. 1987). A spectral index α=$-$0.75 agrees with that of the dereddened UV continuum of Mkn 79 (Oke & Zimmerman 1979; Tsvetanov & Yancoulova 1989). The photoionization model results are shown in Fig.2 together with the observed line ratio at different distances from the centre.

Applying the relation between [OIII]/[OII] and U shown in Fig.1 to our data at PA=12^o we obtain U$\propto$R$^{-0.7\pm0.2}$ for α=$-$0.75 and U approximately constant with R for α=$-$1.5. Along PA=50^o U$\propto$R$^{-1.5\pm0.2}$ for both spectral indices. These relations imply that the electron density falls with increasing distance along PA=12^o as $N_e\propto$R$^{-1.3\pm0.2}$ for α=$-$0.75 and as $N_e\propto$R$^{-0.5\pm0.2}$ along PA=50^o. Thus the average electron density falls from $\approx$ 600 cm^{-3} at the nucleus to $\approx$ 25 cm^{-3} along PA=12^o, and 160 cm^{-3} along PA=50^o at the some distance of 10 arcsec from the centre. These results are in agreement with the trends suggested by the variation in the density-sensitive [SII]λ6717/λ6731 line ratio along PA=12^o shown in Paper 1. The near constant electron density along PA=50^o suggests that the emission in this direction, which coincides with the stellar bar, may be due to HII regions with average electron densities 10^2–10^3 cm^{-3}.

Overall, the preliminary analysis of both the density-sensitive [SII]λ6717/λ6731 line ratio (Paper 1) and the observed [OIII]/[OII] line ratio suggests a significant decrease in the ENLR gas density with increasing distance along PA=12^o whilst it remains nearly constant in the direction of the stellar bar (PA=50^o).

3. Modelling the ENLR emission lines in Mkn 79

There are several possible mechanisms for the ENLR gas ionization (Viegas et al. 1992 and references therein). The arc-like structures seen in the cones of high-excitation gas in some ENLRs suggests that in addition to photoionization by the central source (Robinson et al. 1987) a photoionizing shock may also be required (Sutherland et al. 1993). There are, however, problems explaining the highest excitation line strengths in these types of model, such as [OIII]λ5007, HeIIλ4686 and [NeV]λ3425 observed in the ENLR of NGC1068 (Nazarova 1995). Evans and Dopita (1986) and Bergeron et al. (1989) modelled the ENLR of NGC1068 with two gas components: HII regions and highly ionized low density gas. They also suggested that the continuum of the central source is strongly absorbed up to 20–60 Ryd. This leads to the conclusion that the intrinsic soft X-ray luminosity of NGC1068 is 2 orders of magnitude larger than that observed.

Recently Binette et al. (1996) proposed that the high-ionization line strengths, together with other problems such as low electronic temperatures and the small range in the HeII/Hβ ratio, could be successfully solved by assuming that the ENLR contains a combination of matter-bounded and ionization-bounded clouds. These two cloud populations have different spectra and therefore their combination can reproduce a wider range of observed ENLR spectra. A principal result of this work was that the ionization-bounded clouds are photoionized by the radiation from the central source which has been attenuated by the matter-bounded component.

In this section we explore the advantages of such multi-component gas models in attempts to fit the observed ENLR spectrum of Mkn 79 at different distances from the centre.

3.1. Multiple gas components

As discussed in Sect. 2, we observe an ENLR density gradient along PA=12^o which would maintain a larger U at greater distance and thereby result in significant line emission. The mere fact that we see line emission at such large distances implies that the continuum flux cannot be absorbed completely close to the nucleus. Taking a homogeneous gas envelope throughout the ENLR with a density gradient $N_e\propto$R$^{-1.3}$, the column density (N_h) at distance R will be

N_h =R N_E=R N_o(R/R$_o$)$^{-1.3}$.

The electron density in the central region with radius R$_o$ $\approx$ 600pc (1 arcsec) is N_e $\approx$ 600 cm^{-3}. At a distance of 10 kpc, this then implies N_h = 5 $\times$ 10^{23} cm^{-2}. This column would strongly

Table 1. Observed line fluxes relative to Hβ and 1σ errors along PA=12^o

Ion λ	Region 1	Region 2	Region 3	Region 4	Region 5	Region 6	Region 7	Region 8
[OII] 3726,3729	1.83±0.26	1.92±0.18	2.11±0.17	1.95±0.17	2.47±0.26	2.31±0.22	1.55±0.20	0.85±0.15
Hβ	1	1	1	1	1	1	1	1
[OIII] 4959,5007	4.88±0.72	4.68±0.49	7.03±0.44	11.92±0.4	10.7±1.06	3.63±0.54	1.65±0.1	0.72±0.14
[NII] 6548,6583	3.73±0.6	2.87±0.33	2.57±0.18	3.14±0.2	5.7±0.66	3.18±0.45	1.72±0.28	1.69±0.28
[SII] 6717,6731	1.33±0.13	1.28±0.09	0.94±0.07	1.0±0.07	2.0±0.25	1.14±0.15	0.85±0.2	0.79±0.16
Distance (kpc)	9.45	6.93	4.41	1.89	1.89	4.41	6.93	9.45
Size (kpc×kpc)	0.94×2.52	0.94×2.52	0.94×2.52	0.94×2.52	0.94×2.52	0.94×2.52	0.94×2.52	0.94×2.52
L(Hβ) (10^{38}erg s^{-1})	0.57	2.7	6.8	104.4	16.9	2.2	1.04	0.78
N_e([SII]) (cm^{-3})	<80	80	254	652	80	<80	<80	<80
M_{gas} ($10^3 M_\odot$)	<0.17	0.44	1.1	18.5	1.5	<0.62	<0.28	<0.22
F(Hβ)$^{(a)}$	2.84 ±0.3	13.5±1.0	34.0±7.2	522.1±16	134.4±13	11.25±1.1	5.2±0.6	3.9±0.5
F(Hβ)$^{(b)}$	2.67±0.3	12.7±0.9	31.9±6.7	490.3±15	126.2±12	10.56±1.0	4.9±0.6	3.7±0.5

(a) Observed flux of narrow component of Hβ in units of 10^{-17}erg s^{-1}cm^{-2} (see text for details)
(b) Flux of narrow component of Hβ from 1 cm^{-2} at the emitting surface in units of 10^{-6}erg s^{-1}cm^{-2}

Table 2. Observed line fluxes relative to Hβ and 1σ errors along PA=50^o

Ion λ	Region 1	Region 2	Region 3	Region 4	Region 5	Region 6	Region 7	Region 8
[OII]3726,3729	2.21±0.41	1.8±0.31	2.41±0.24	2.21±0.11	2.61±0.22	2.09±0.29	0.96±0.11	1.12±0.10
Hβ	1	1	1	1	1	1	1	1
[OIII] 4959,5007	0.51±0.01	1.33±0.21	4.86±0.47	11.72±0.6	9.49±0.89	3.93±0.61	0.41±0.12	0.41±0.12
[NII] 6548,6583	1.97±0.36	2.67±0.35	2.65±0.28	3.84±0.38	4.9±0.78	3.17±0.46	1.66±0.15	2.25±0.2
[SII]6717,6731	1.01±0.15	1.14±0.17	1.08±0.17	0.84±0.08	1.65±0.19	1.2±0.21	0.68±0.14	0.86±0.11
Distance (kpc)	9.45	6.93	4.41	1.89	1.89	4.41	6.93	9.45
Size (kpc×kpc)	0.94×2.52	0.94×2.52	0.94×2.52	0.94×2.52	0.94×2.52	0.94×2.52	0.94×2.52	0.94×2.52
L(Hβ) (10^{38}erg s^{-1})	1.98	2.52	4.96	80.7	22.3	2.7	0.65	0.67
N_e([SII]) (cm^{-3})	<80	84	250	636	80	<80	<80	<80
M_{gas} ($10^3 M_\odot$)	<0.57	0.74	1.45	13.1	3.6	0.44	<34	<0.35
F(Hβ)$^{(a)}$	9.9±1.2	12.6±1.4	24.8±2.2	403.7±20	111.7±9.4	13.7±1.8	32.5±2.1	33.6±1.8
F(Hβ)$^{(b)}$	9.3±1.1	11.8±1.3	23.3±2.1	379.0±19	104.9±8.8	12.8±1.7	30.5±1.9	31.5±2.0

(a) Observed flux of narrow component of Hβ in units of 10^{-17}erg s^{-1}cm^{-2} (see text for details)
(b) Flux of narrow component of Hβ from 1 cm^{-2} at the emitting surface in units of 10^{-6}erg s^{-1}cm^{-2}

absorb the continuum resulting in a low electron temperature ($<$ 4000K) at large distance. Therefore a homogeneous gas envelope with a density gradient falling off from the nucleus cannot produce the observed strong line emission at large distances. However, it seems unrealistic to suggest that there does not exist some low density gas filling most of the ENLR, as is found in the galactic interstellar medium. Therefore, following Binette et al. (1996), we will assume two gas components: a system of high density clouds and a low density gas envelope. The low density gas absorbs the incident continuum from the nucleus, transmitting an attenuated continuum. The low density gas also emits a diffuse continuum, and these two continua illuminate the high density clouds.

3.2. Models A and B

3.2.1. The ionizing continuum

The shape of the nuclear continuum in Mkn 79 has been derived from several sources. The UV continuum corrected for reddening was taken from Oke & Zimmerman (1979), approximated as a powerlaw continuum with $\alpha = -0.75$. The X-ray continuum in the 2 keV−10 keV range was assumed from Turner & Pounds (1989). The rest of the continuum shape was taken to follow that of the canonical AGN continuum given in CLOUDY (Mathews & Ferland, 1987). The adopted shape of the nuclear continuum in Mkn 79 used in our study is shown in Fig.2 together with the canonical AGN continuum provided in CLOUDY.

In Paper 1 we estimated the number of photons in the assumed power-law central continuum to be 1.2×10^{51}photons s^{-1}, assuming no reddening correction and 4.7×10^{53}photons s^{-1} assuming the reddening corrected con-

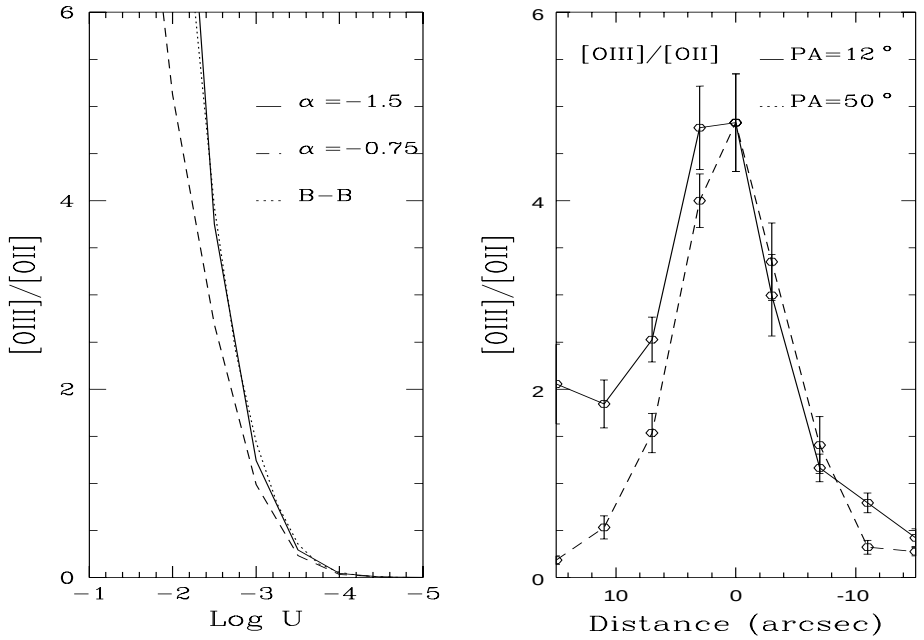

Fig. 1. The theoretical [OIII]/[OII] line ratio versus Log U and the observed line ratio in Mrk79 at different distances from the centre. See text for details.

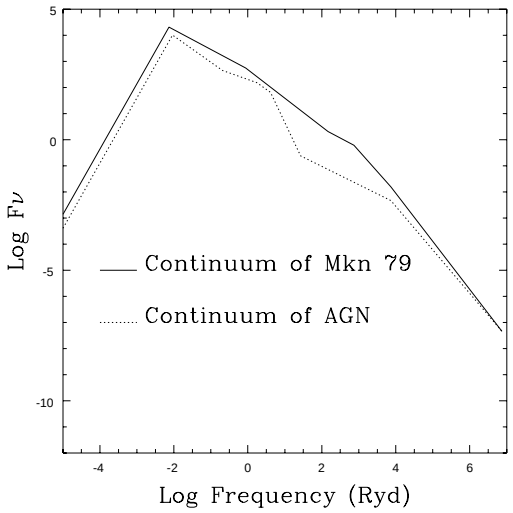

Fig. 2. The adopted continuum of Mkn 79 compared to the canonical AGN continuum provided in CLOUDY. Both continua are plotted in units of Photons Ryd^{-1} cm^{-2} s^{-1} with arbitrary offsets.

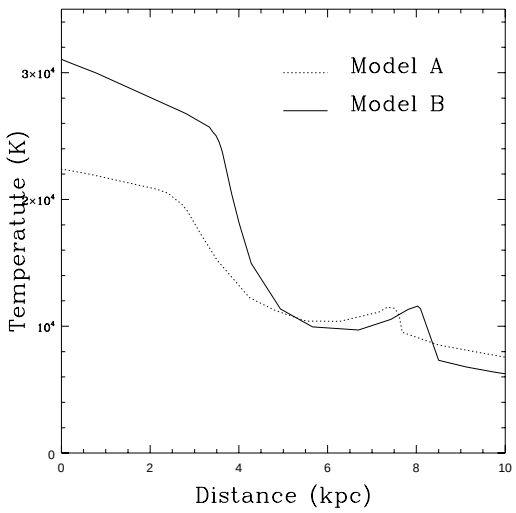

Fig. 3. The electron temperature profiles for homogenous envelopes of low density gas with densities as in Models A and B.

tinuum of Oke & Zimmerman (1979) who took E(B−V) = 0.22. We therefore calculated two models within this luminosity range: Models A and B with nuclear luminosities of 6.6×10^{51}photons s^{-1} and 6.6×10^{52}photons s^{-1} respectively, both with the continuum shape shown in Fig.2. The corresponding ionizing photon fluxes at the starting radius of the ENLR (allowing for attenuation by gas in the nucleus, Sect. 3.2.2) are 1.5×10^{8} photons cm^{-2} s^{-1} (Model A) and 1.5×10^{9} photons cm^{-2} s^{-1} (Model B) and the ionization parameter Log U=−1.5 (Model A) and Log U=−1.0 (Model B). The starting radius has been taken as 630pc corresponding to the inner radius of regions 4 and 5 which are closest to the nucleus. It should be noted that Models A and B have different densities for the low density gas.

3.2.2. Technique

All calculations were carried out using CLOUDY applied for plane-parallel slab of gas. We assumed solar abundances in all our calculations although we explored the influence of a nitrogen abundance 1.5 times higher than solar (Sect. 3.5).

The aim of this study was to calculate the line fluxes as a function of distance from the central source, taking into account the attenuation of the ionizing continuum by gas at smaller radii. Thus the transmitted portion of the incident continuum and the

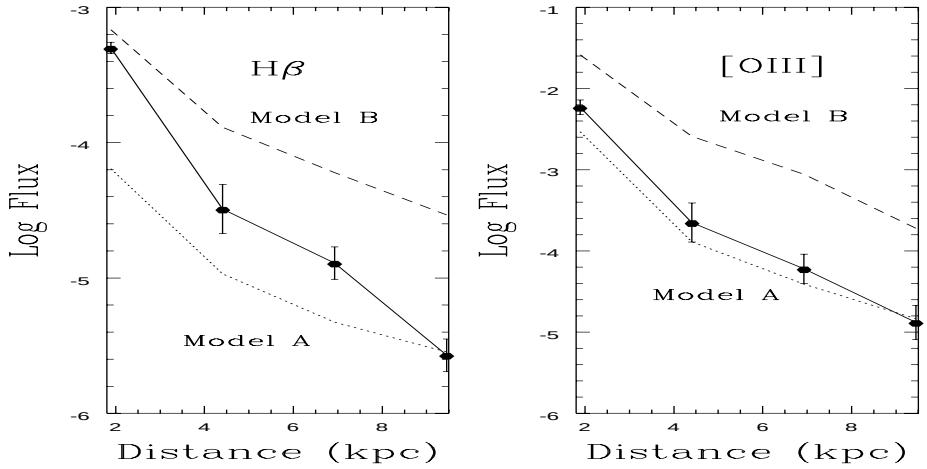

Fig. 4. The observed and predicted fluxes of the Hβ and [OIII]λ5007 lines for the low density gas allowing for attenuation of the ionizing continuum (in units of erg cm^{-2} s^{-1} at the ENLR).

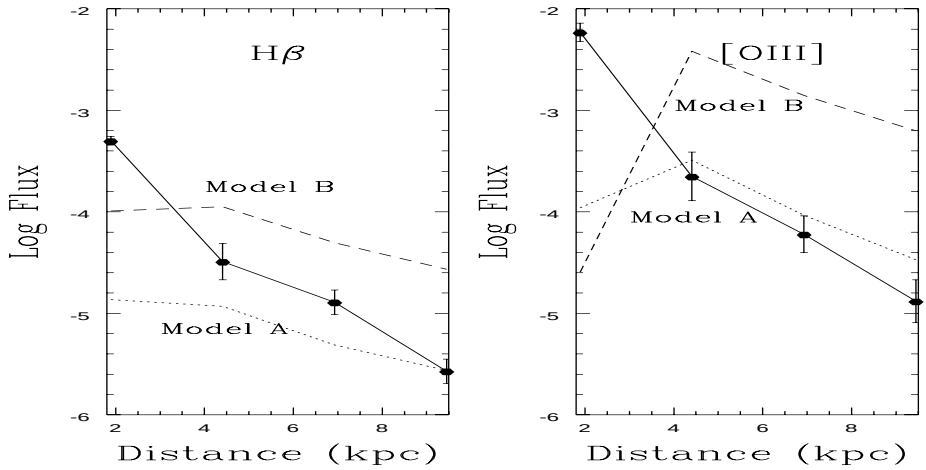

Fig. 5. The observed and predicted fluxes of the Hβ and [OIII]λ5007 lines for the low density gas assuming no attenuation of the ionizing continuum (in units of erg cm^{-2} s^{-1} at the ENLR).

diffuse continuum emitted by the low density gas were calculated for Models A and B as a function of distance from the centre, where the incident continuum for a given region is the sum of the transmitted and diffuse continua from the previous region. The only exception to this method was for the inner regions 4 and 5. For the inner ENLR we need to adjust the intrinsic nuclear continuum of Mkn 79 shown in Fig.2 to allow for attenuation by gas closer to the nucleus (i.e. within 1 arcsec). It is highly unlikely that the nuclear continuum will have suffered no attenuation over this distance. To simulate attenuation by nuclear gasand thereby provide an incident continuum at the inner radius of the ENLR, the AGN nuclear continuum was first passed through a column of low density gas equal to that corresponding to half of the path length through region 4 ($\sim 10^{21}$ cm^{-2}). The resulting transmitted continuum was then taken as the incident continuum at the starting radius of each model. The values of U and photon flux at the starting radius take this attenuation into account. Although the effect is small on U and the photon flux, the shape of the continuum has a significant effect on the emission line spectrum as we describe in the next section.

3.3. Low density gas

The low temperature predicted by photoionization models has been discussed in several papers (Binette et al. 1996 and references therein). We show in Fig. 3 the electron temperature profiles for homogeneous gas envelopes of low density gas with the densities used in Models A and B. The temperature remains high at large distances, and therefore we expect strong high ionization line emission, such as [OIII]λ5007, at distances up to 8 arcsec or greater. The observed and model fluxes of the Hβ and [OIII]λ5007 lines in units of erg cm^{-2} s^{-1} for the ENLR are shown in Fig.4. Although 1σ errors are presented in Tables 1, 2, and 3, obtained by fitting gaussian profiles using the TWODSPEC spectral analysis software (Wilkins & Axon 1994), we show 3σ error-bars in Figs. 4, 5 and 9 to permit the realistic comparison between observation and model.

The Model A Hβ and [OIII]λ5007 line fluxes follow the general trend of the observations. However, the absolute values are too small even for a filling factor of unity. For Model B the calculated line fluxes fit the observations reasonably well if we assume a low density gas filling factor of about 0.1. However we cannot simultaneously fit the low ionization [OII]λ3727, [NII]$\lambda\lambda$6548,6583 and [SII]$\lambda\lambda$6717,6731 lines with the low

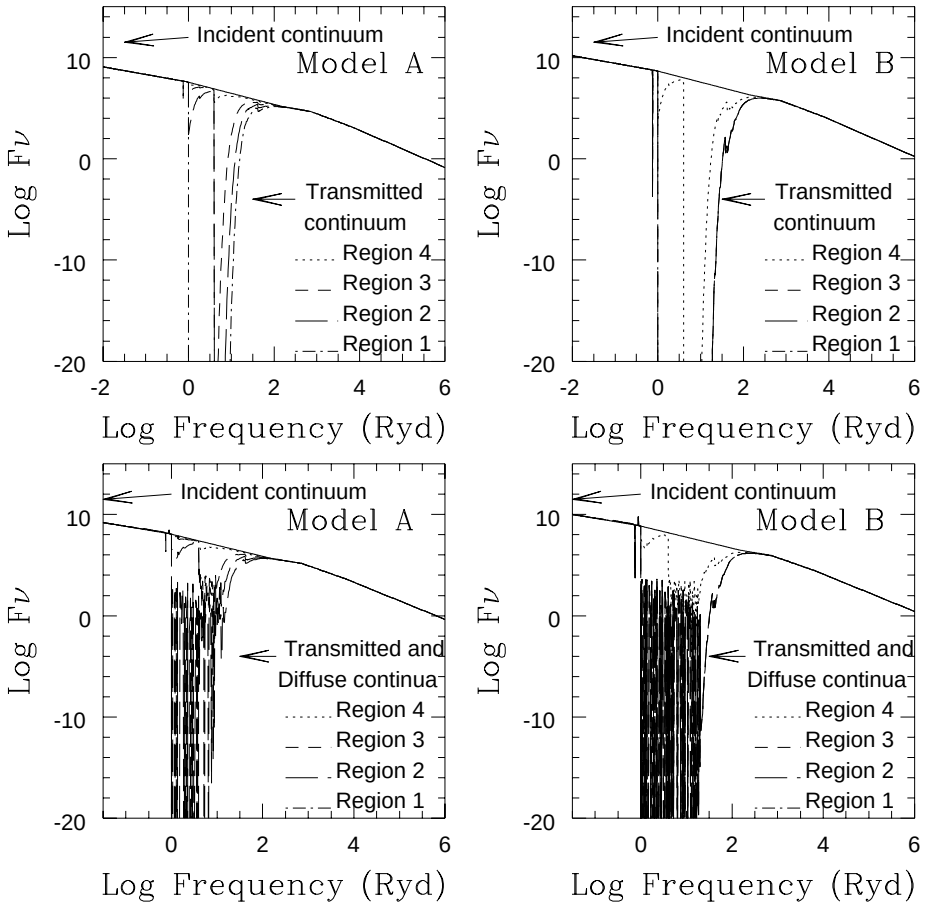

Fig. 6. The unattenuated nuclear (incident) continuum together with the transmitted continua (top row) and the sum of the transmitted and diffuse continua (bottom row) for regions 1–4 in Models A and B. The continua are in units of Photons Ryd^{-1} cm^{-2} s^{-1} with an arbitrary constant added to each for display purposes.

density gas. These lines are very weak in the regions close to the nucleus in both models, contrary to the observations.

The influence of the attenuated continuum on the line flux for the low density gas is illustrated in Fig.5. Here we did not include the effect of attenuation with distance from the nucleus, but took into account only the distance of each region. In Fig.5 the line fluxes for those regions located closest to the nucleus are very small contrary to the observations. This problem cannot be overcome by combining with the high density gas component (Sect. 3.4) since the effect occurs for such gas as well, and is due to intense ionization by the AGN continuum close to the centre.

3.4. High density gas

Since the low and high ionization line emission from the ENLR of Mkn 79 cannot be explained simultaneously by a single low density gas component, we next included the emission from high density gas clouds which were assumed to be distributed within the low density gas envelope.

The emission from high density gas was calculated for regions 1–4 located at different distances from the centre along PA=12^o. The calculations were performed for each region using the attenuated continua from smaller radii. The shape of the unattenuated nuclear (incident) continuum, the transmitted continua and the sum of the transmitted and diffuse continua for regions 1–4 for both models are shown in Fig.6. It should be noted that the shape of the sum of the transmitted and diffuse continua is quite different from the transmitted continuum alone. Adding the diffuse continua reduces the depth of the gap in the continuum between approximately 1 and 100 Ryd. The emission of the high ionization [OIII]$\lambda\lambda$4959, 5007 lines depends on the shape of the continuum in this region as it controls the parent ion population.

The flux of the [OII]$\lambda\lambda$3726,3729, [OIII]$\lambda\lambda$4959,5007, [NII]$\lambda\lambda$6548,6583 and [SII]$\lambda\lambda$6717,6731 doublets for different electron densities in Models A and B are presented in Fig.7 and Fig.8. The fluxes of the lines for the low density gas in the final composite model are shown as the solid line. For Model A the lines fluxes decrease with distance from the centre for all gas densities plotted, whereas for Model B the low ionization lines of [OII], [NII] and [SII] are less intense in the low density gas near to the centre compared to the more distant regions. This effect is due to the higher photon density and hence higher degree of ionization at small distances in Model B.

3.5. Composite models of the ENLR

The line fluxes calculated with different densities for regions 1–4 have been combined in order to obtain the best fit to the observed line ratios and line fluxes. The best fit for the 4 line ratios (relative to Hβ) for both models are shown to-

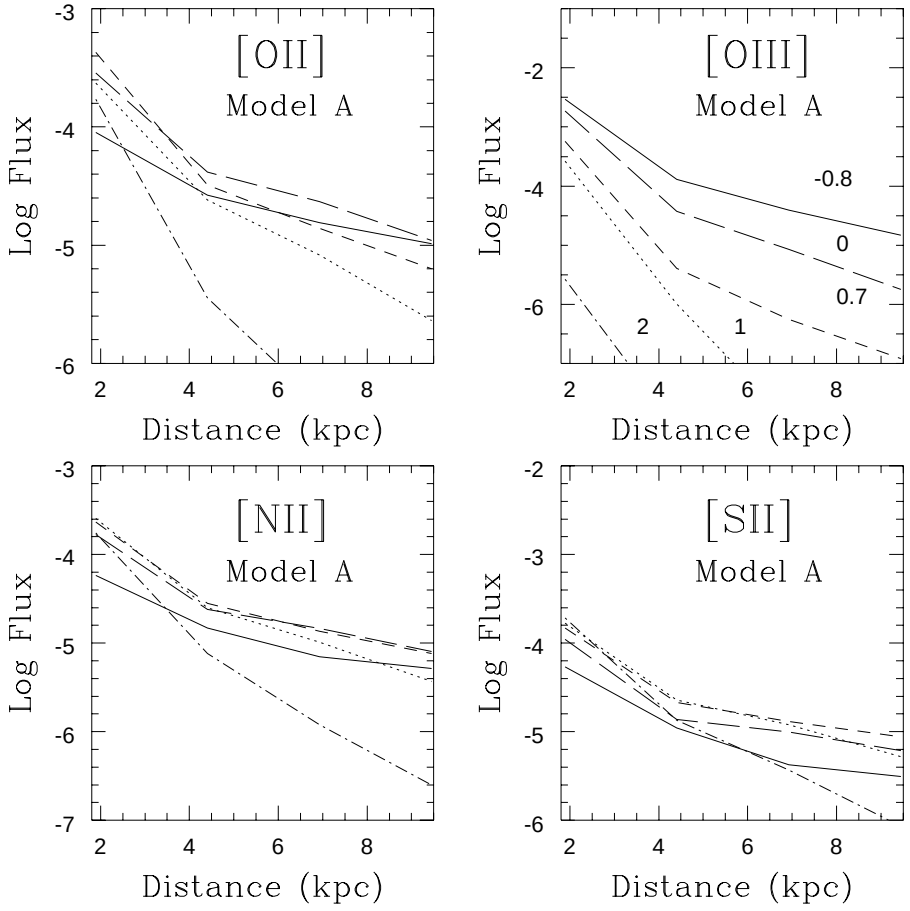

Fig. 7. The theoretical fluxes of the [OII], [OIII], [NII] and [SII] doublets at different distances from the centre for Model A (in units of erg cm^{-2} s^{-1} at the ENLR).The fluxes of the lines for the low density gas are shown as the solid line. The numbers on the [OIII] loci correspond to the logarithm of the electron densities (Log N$_e$).

gether with the observed values in Fig.9, and the numerical results are presented in Table 3. We tabulate the model line ratios (relative to Hβ) for [OII]$\lambda\lambda$3726,3729, [OIII]$\lambda\lambda$4959,5007, [NII]$\lambda\lambda$6548,6583 and [SII]$\lambda\lambda$6717,6731 together with the predicted Hβ flux (F(Hβ)$_{pred}$ at the ENLR) for the different regions. Table 3 also gives the relative contributions of the high (HDG) and low (LDG) density gas (HDG/LDG) to the Hβ flux, their densities (Log N$_e$(LDG) and Log N$_e$(HDG)), the cumulative column density at the outside of that region (Log (N$_h$)), the average electron density and the filling factor for each region. The filling factor was estimated by comparison of the observed and predicted Hβ flux. The observed Hβ flux (F(Hβ)$_o$ at the ENLR) are shown at the bottom of Table 3.

In practice, the modelling was performed in two stages. After an inital calculation we derived parameters such as the column density at different distances from the centre and the relative contributions from the low and high density gas. These values were then used to recalculate the sum of the transmitted and diffuse continua for each region and hence the line fluxes. The second iteration used the corrected (attenuated) continua, which are important for the regions distant from the nucleus.

For Model A, despite the fact that the line ratios relative to Hβ can be made to agree with the observations along PA=12^o to within 3 σ, the model Hβ fluxes in regions 3 and 4 are factors of 18 and 2 times smaller than observed. Hence the column density and filling factor are not quoted for this model. Since Model A cannot predict the observations it is therefore ruled out.

The Model B line ratios are in good agreement with the observations to within 3 σ for all lines except [NII]. Disagreements between the theoretical and observed [NII]/Hβ line ratios have been commented on in several previous studies. For example, Simpson & Ward (1996) modelled the NLR in a sample of AGNs and found that the predicted [NII]/Hβ line ratio is much smaller than is seen in most objects. They discussed some possibilities to explain this effect, one of which is a higher than solar nitrogen abundance, as a result of processing by an early generation of massive stars. To investigate this possibility we computed several theoretical models with nitrogen abundences in excess of solar. A good fit to the observed [NII]/Hβ line ratio was obtained with an N/H ratio about 1.5 times solar. Since estimates of abundances in AGN are very uncertain, we choose to present results for models with solar metal abundances.

For Model B the filling factor decreases with distance from the centre, but is still high enough to provide sufficiant attenuation of the ionizing continuum. The average electron density derived from Model B decreases with distance as R$^{-1.4}$, in good agreement with the analysis obtained from the [OIII]/[OII] line ratio presented in Sect. 2.

In Paper 1 we discussed the ionizing photon budget and concluded that the total Hβ flux for Mkn 79 could not be explained

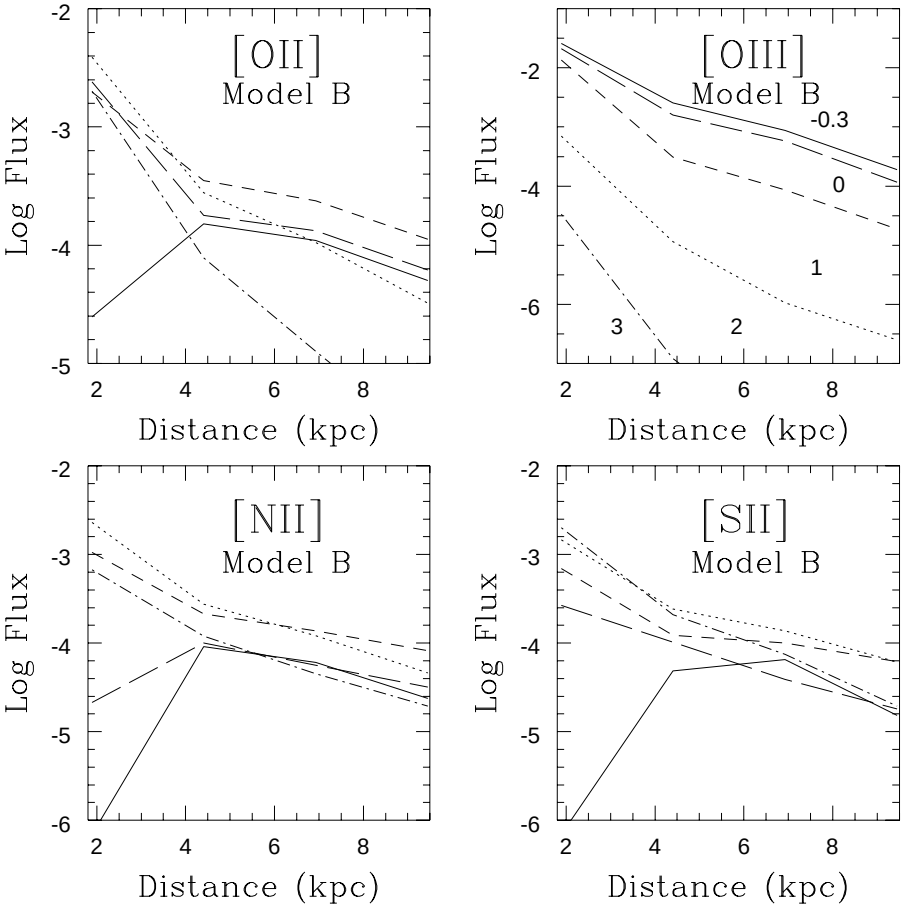

Fig. 8. The theoretical fluxes of the [OII], [OIII], [NII] and [SII] doublets at different distances from the centre for Model B (in units of erg cm^{-2} s^{-1} at the ENLR). The fluxes of the lines for the low density gas are shown as the solid line. The numbers on the [OIII] loci correspond to the logarithm of the electron densities (Log N_e).

by a spherical gas system illuminated by the observed ionizing continuum. Here we have found that the continuum flux for Model B, which is consistent with that of the dereddened nuclear ionizing continuum, can explain the observed ENLR emission. These two findings are not in disagreement, as the calculation in Paper 1 included the Broad Line Region (BLR) Hβ flux, and was therefore simply an illustration of the well known BLR energy-budget problem (Netzer 1985).

4. The extended continuum in Mkn 79

In Paper 1 we showed that the observed ENLR spectra of Mkn 79 in the two position angles also show an extended continuum. along PA=50^o, which coincides with the stellar bar, the ENLR continuum spectrum resembles an ordinary stellar population. However along PA=12^o, the ENLR in the direction of the radio jet, there is an additional blue continuum at all distances from the centre. A sample of the ENLR spectra along the two position angles are replotted in Fig.10 together with the difference spectra. These difference spectra show the extended blue continuum, assuming the same stellar spectrum in both position angles. The observed nuclear flux at 4000Å from Paper 1 is $\approx 5\times10^{-15}$ erg cm^{-2} s^{-1}Å^{-1}. The extended blue continuum fluxes along PA=12^o range from 3–5$\times10^{-17}$ erg cm^{-2} s^{-1}Å^{-1} for Regions 1–3, and are similar for regions 5–8. The continua for regions 4 and 5 are badly contaminated by nuclear light due to seeing effects (Paper 1), but for the other more distant regions the extended blue continuum is about 1 percent of the nuclear continuum.

There are several possible sources of the extended blue continuum at large distances from the centre. These include star-formation regions, a nebula continuum, photoionization by shock or a reflected nuclear continuum scattered in the ENLR gas. In this section we compare the predictions of these various emission mechanisms.

4.1. Star-formation regions

The colour of the extended blue continuum and the extended [OIII]λ5007 line emission along PA=12^o are similar to that expected from star-formation regions. However the optical broadband CCD images of Mkn 79 (Mazzarella & Boroson 1993) (see Fig.1, Paper 1) show that Mkn 79 has an ordinary spiral structure with an inner ring of HII regions located about 15 arcsec from the centre, and with a bar elongated along PA=50^o. There are no noticable knots inside 15 arcsec along PA=12^o like those seen in regions with large OB star associations. Therefore it seems unlikely that the extended blue continuum and line emission along PA=12^o can be explained by star-formation.

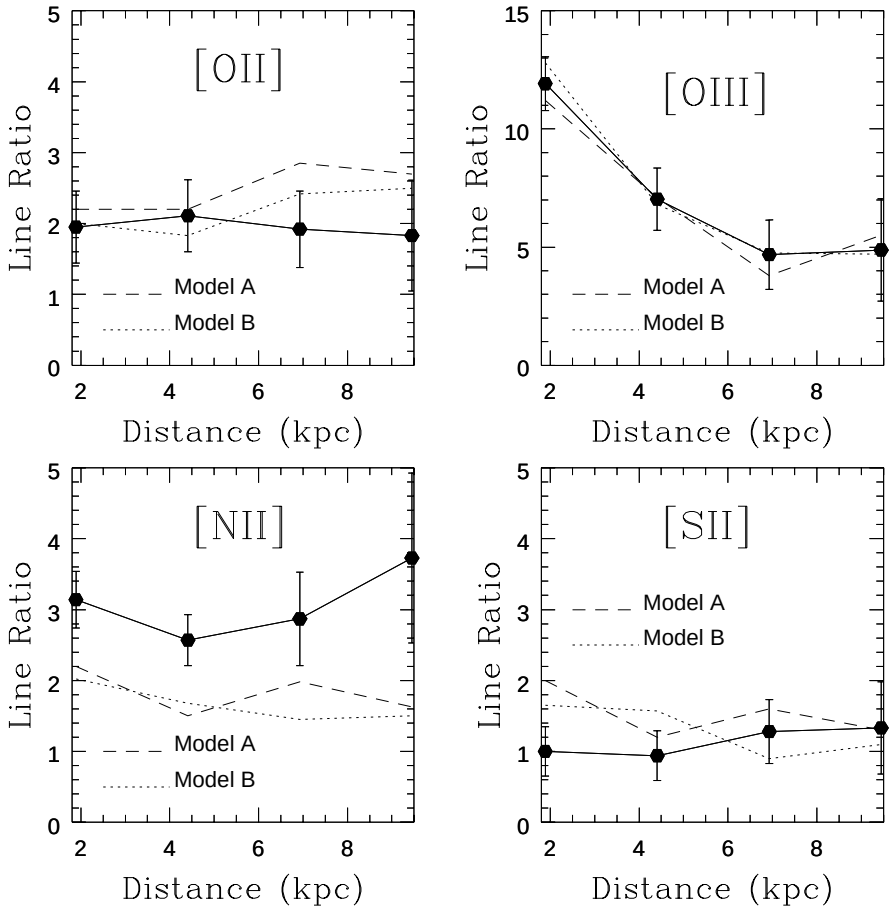

Fig. 9. The theoretical and observed line ratios relative to Hβ for the [OII], [OIII], [NII] and [SII] doublets at different distances from the centre. The dashed line corresponds to Model A and the dotted line to Model B.

4.2. Nebular continuum

The UV continuum of Mkn 79 (Oke & Zimmerman 1979) shows the hydrogen Balmer continuum edge at 3646Å, and the extended blue continuum could in principal be due to emission from free-free and bound-free nebular continuum and two-photon decay. For the nebular continuum the ratio of the continuum luminosity integrated over the range 3700–5230Å to the Hβ luminosity is $\approx$1.5, assuming Case B recombination for gas at T_e=10^4K (Osterbrock 1989). This ratio does not depend strongly on T_e, rising for example to 2.1 for T_e=2×10^4K. The observed luminosity of the extended blue continuum to Hβ is about two orders of magnitude higher than these values. This discrepancy cannot be removed by dereddening given that the extended blue continuum extends shortward of Hβ. In any case, we show in Paper 1 that the narrow line Balmer decrement is nearly constant at all distances from the nucleus and along both position angles. It has an average value of about 3.1 corresponding to pure case B recombination. Thus, the extended blue continuum cannot be explained by nebular continuum emission.

4.3. Reflected continuum in the ENLR

Electrons or dust in the ENLR could reflect some of the nuclear continuum into our line of sight (Heckman et al. 1995; Cid Fernandes & Terlevich 1995; Tran 1995). As Model B provides a good fit to the observed line fluxes, it is interesting to see how much reflected continuum it would produce. For this model the cumulative column density in the direction of the ENLR is $\approx 4\times10^{21}$ cm^{-2} for region 1, and slightly less for the closer regions (Table 3). We have used CLOUDY to calculate the reflected continuum for these column densities, and the results are shown in Fig.11. The theoretical reflected continuum is 2–3 percent of the nuclear (incident) AGN continuum.

To make a detailed comparison between the strength of the observed extended blue continuum and the theoretical reflected continuum we need to take into account the geometry of the ENLR gas which we used in the modelling process. For a plane-parallel slab the reflected continuum is emitted from the illuminated face of the cloud back in the direction of the incident continuum (i.e. into 2π sr). So, the proportion of the reflected continuum in the direction to the observer could change from $\sim$ 0.5 (when the ENLR is located in the plane of the sky) to 0 (when we see the nucleus through the ENLR). The optical images imply that the galaxy disk, and therefore presumably the ENLR gas, is close to the plane of the sky. The ENLR might be slightly inclined given that the extended emission is more prominent in the north than the south. Thus we expect that the portion of the reflected continuum in the direction to the observer will be about 0.5 or slightly less. Taking this factor into account gives a predicted reflected to nuclear continuum ratio

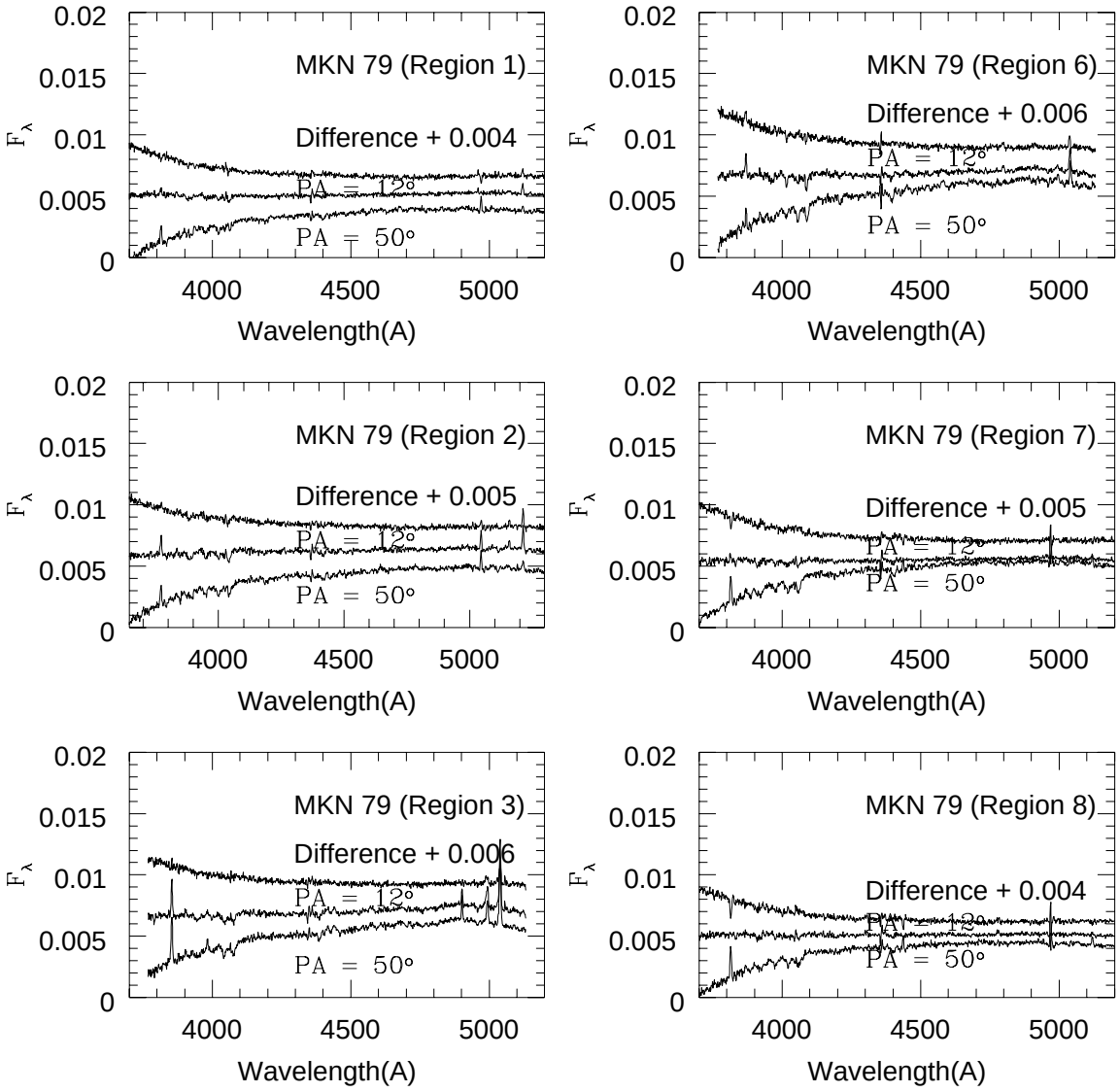

Fig. 10. The observed extended continua along the two position angles (in units of 10^{-14} erg s^{-1} cm^{-2} Å^{-1}) together with the difference between them (the extended blue continuum).

of about 1 percent, which consistent with the observed extended blue continuum. Thus, Model B appears capable of explaining both the ENLR line and extended blue continuum emission in Mkn 79 along PA=12^o.

5. Conclusions

We have modelled the observed ENLR along PA=12^o in Mkn 79 with two gas components, comprising a system of high density clouds embedded in a low density gas envelope. The low density gas at small radii attenuates the incident continuum from the AGN, altering its shape and producing a diffuse continuum. These two continua then illuminate the more distant low and high density gas. The emission lines emitted from both the low and high density gas are combined to produce a theoretical emission line spectrum for comparison with observations.

Two models were constructed with different values for the nuclear continuum luminosity and the density of the low density gas component. For Model A with a central source luminosity of 6.6×10^{51}photons s^{-1}, the line ratios (relative to Hβ) coincide well with the observations, but the absolute flux of Hβ is too low at large distances. Model B has a central source luminosity of 6.6×10^{52}photons s^{-1}, consistent with the dereddened nuclear continuum. The combined line fluxes emitted by the low and high density gas in this model provide a good fit to both the line ratios and Hβ flux for both the low and high ionization lines throughout the ENLR over distances up to 10 kpc from the nucleus.

Model B was then used to predict the strength of the reflected continuum from the ENLR, and this was found to be consistent with the observed extended blue continuum along PA=12^0. Thus Model B fits both the ENLR line fluxes and the extended blue

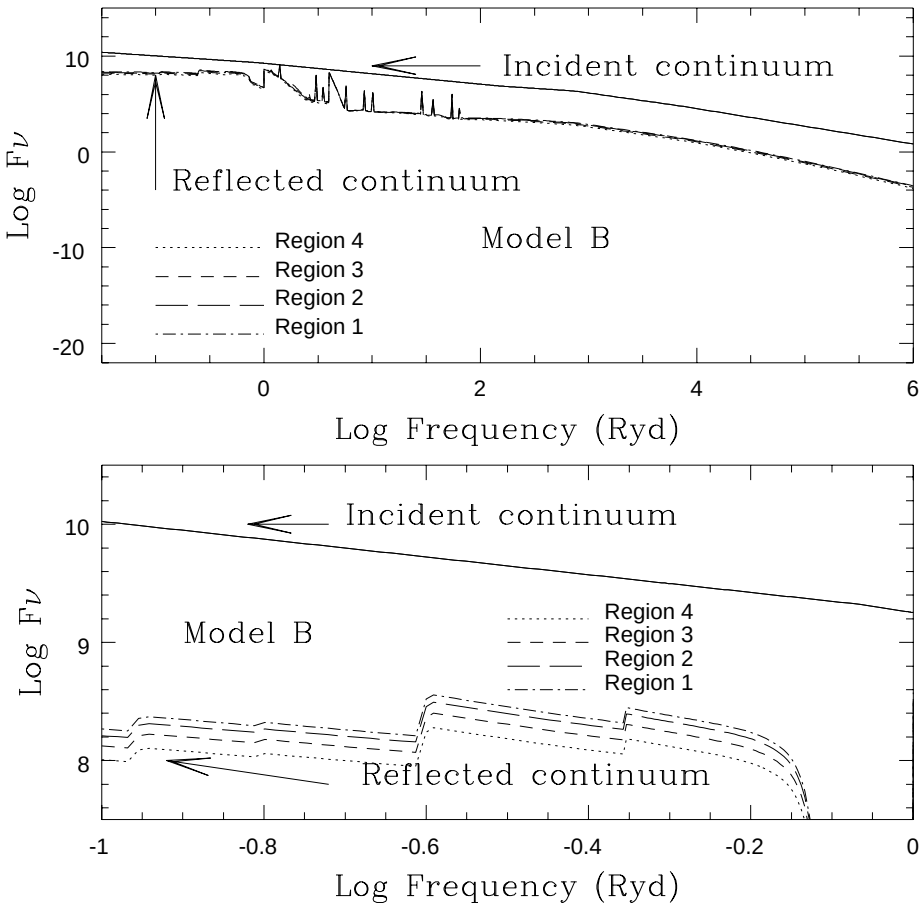

Fig. 11. The unattenuated nuclear (incident) continuum and the reflected continuum from Model B (in units of Photons Ryd^{-1} cm^{-2} s^{-1} plotted with an arbitrary offset). The lower box shows an expanded view of the UV–optical region.

Table 3. Predicted line fluxes relative to Hβ for Model A and Model B.

	Region 1 Model A	Region 1 Model B	Region 2 Model A	Region 2 Model B	Region 3 Model A	Region 3 Model B	Region 4 Model A	Region 4 Model B
[OII]	3.6	2.5	2.85	2.42	2.22	1.83	2.2	2.0
[OIII]	5.1	4.7	3.83	4.76	7.1	6.8	11.2	12.8
[NII]	1.8	1.5	1.98	1.45	1.5	1.68	2.2	2.0
[SII]	1.0	1.1	1.6	0.9	1.2	1.57	2.3	1.65
Log F(Hβ)$_{pred}$	−5.41	−4.37	−4.99	−3.78	−5.74	−3.71	−3.58	−3.13
HDG/LDG	0	0.5	1	3.3	0.6	2	3	2
LogN$_e$(HDG)	0	0	0.7	1.0	1	2.0	2	3.0
LogN$_e$(LDG)	−0.8	−0.3	−0.8	−0.3	−0.8	−0.3	−0.8	−0.3
Log (N$_h$)		21.42		21.36		21.27		21.15
N$_e$ (cm^{-3})		0.1		1		16.5		720
Filling factor		0.1		0.1		0.25		1
Log F(Hβ)$^{(b)}$	−5.57		−4.89		−4.49		−3.31	

(b) Flux of narrow component of Hβ from 1 cm^{-2} at the emitting surface.

continuum in Mkn 79, showing that multi-component narrow line regions provide a good basis for modelling.

Acknowledgements. One of us (L.N.) wish to thank the University of Leicester for their hospitality. This work has been supported by an SPSL grant. We would also like to thank Gary Ferland for providing a copy of CLOUDY and referee F.Durret for useful comments. The calculations were performed on SUN and DEC workstations provided by the PPARC Starlink project at Leicester.

References

Antonucci R.R.J., 1993, ARA&A, 31, 473
Antonucci R.R.J. & Miller J.S., 1985, ApJ, 297, 621
Binette L., Wilson A.S. & Storchi-Bergmann T., 1996, A&A (in press)
Baldwin J.A., Phillips M.M. & Terlevich R.J., 1981, PASP, 93, 5
Bergeron J., Petitjean P. & Durret F., 1989, A&A, 213, 61
Colina L., 1992, ApJ, 386, 59
Sid Fernandes R.Jr & Terlevich R, 1995, MNRAS, 272, 423
Evans N. & Dopita M.A., 1986, ApJ, 310, L15-L19
Haniff C.A., Ward M.J., Wilson A.S., 1991, ApJ, 368, 167
Heckman T., Krolick J., Meurer G., Galzetti D., Kinney A., Koratkar A., Leitherer C., Robert C. & Wilson A., 1995, ApJ, 452, 549H
Ferland G.J., 1991, Internal Report 91-01,OSU Astron. Dep.
Mazzarella J.M. & Boroson T.A., 1993, ApJS, 85, 27
Mathews W.G., Ferland G.J., 1987, ApJ,323, 456
Nazarova L.S.,O'Brien P.T. & Ward M.J., 1996, A&A, 307,365
Nazarova L.S., 1995, A&A, 299,359
Netzer, H., 1985, MNRAS, 216, 63
Osterbrock D.E., 1989, Astrophysics of Gaseous Nebulae and Active Galactic Nuclei, University Science Books
Oke J.B. & Zummerman B., 1979, ApJ, 231, L13-L17
Oke, J.B. & Lauer, T.R., ApJ, 230, 360
Pogge R.W., 1988, ApJ, 332, 702
Penston M.V., Robinson A., Alloin D.,et al., 1990, A&A, 236, 53
Pogge R.W. & De Robertis M.M., 1993, ApJ., 404, 563
Robinson A., Binette L., Fosbury R.A.E., Tadhunter C.N., 1987, MNRAS, 227, 97
Simpson C. & Ward M.J., 1996, MNRAS (in press)
Sutherland R.S.,Bicknell G.V., Dopita M.A.,1993, ApJ 414,510
Tsvetanov Z.I. & Yancoulova 1989, MNRAS, 237, 707
Tran H.D., 1995, ApJ, 440, 597
Turner T.J., Pounds K.A., 1989, MNRAS, 239, 833
Veilleux S. & Osterbrock D.E., 1987, ApJS,63,295
Viegas S.M, de Gouveia Dal Pino E.M., 1992, ApJ, 384,467
Wilkins T.W. & Axon D.J., 1994, Starlink User Note No. 16
Wilson A.S., Ward M.J., Haniff C.A., 1988, ApJ, 334, 121
Wilson A.S & Tsvetanov Z.I., 1994, AJ, 107, 4, 1227
Whittle M., Pedlar A., Meurs E.J.A., Unger S.W., Axon D.J. & Ward,M.J., 1988, ApJ, 326, 125
Unger S.W, Pedlar A., Axon D.J., et al., 1987, 319, 105

This article was processed by the author using Springer-Verlag LaTeX A&A style file *L-AA* version 3.